



Nonequilibrium phases of a Fermi gas inside a cavity with imbalanced pumpingXiaotian Nie ^{1,2} and Wei Zheng ^{1,2,3,*}¹*Hefei National Laboratory for Physical Sciences at the Microscale and Department of Modern Physics, University of Science and Technology of China, Hefei 230026, China*²*CAS Center for Excellence in Quantum Information and Quantum Physics, University of Science and Technology of China, Hefei 230026, China*³*Hefei National Laboratory, University of Science and Technology of China, Hefei 230088, China*

(Received 20 July 2023; accepted 13 October 2023; published 30 October 2023)

In this work we investigate the nonequilibrium dynamics of one-dimensional spinless fermions loaded in a cavity with imbalanced pumping lasers. Our study is motivated by previous work on a similar setup using bosons, and we explore the unique properties of fermionic systems in this context. By considering the imbalance in the pumping, we find that the system exhibits multiple superradiant steady phases, a bistable regime, and an unstable phase. Furthermore, by making use of the hysteresis structure in the bistable regime, we propose a unidirectional topological pumping. Unlike the usual topological pumping in which the driving protocol breaks time-reversal symmetry, the driving protocol can be time-reversal invariant in our proposal.

DOI: [10.1103/PhysRevA.108.043312](https://doi.org/10.1103/PhysRevA.108.043312)**I. INTRODUCTION**

Ultracold atomic gases coupled to optical cavities provide a versatile platform for studying quantum many-body physics. On the one hand, cavity photons mediate long-range interactions between atoms inside a cavity, which can lead to new phases of atom-cavity hybridized systems. On the other hand, the leaking of the photons from the cavity provides a dissipation channel that will drive the system away from equilibrium, exhibiting rich dynamics and providing a way to detect them. One typical setup involves atoms loaded into a cavity, which is pumped by a pair of counterpropagating pumping lasers. Usually the intensities of the two pumping lasers are balanced, such that they form a standing wave and create a static optical lattice for the atoms. In the past decade, significant advances have been made based on such balanced pumping setups. For example, superradiance of the cavity field has been studied and observed with bosonic [1–15] and fermionic atoms [16–26] inside cavities, respectively. More nonequilibrium dynamical phases without steady states, such as dissipative time crystals which can break discrete or continuous time translation symmetry, have also been predicted [27–37] and observed [38–40] in balanced pumped systems.

Recently, there has been growing interest in exploring the effects of imbalanced pumping lasers on atom-cavity hybridized systems. The intensities of the two counterpropagating lasers can be tuned to be unequal, such that the atoms feel both standing and traveling waves. The asymmetry in the pumping leads to the emergence of novel phases, including distinct superradiant phases and self-organized charge pumping [41,42]. However, though most of the works are focused on the bosonic atoms inside cavities with imbalanced

pumping, the behavior of fermions in this regime remains largely unexplored.

In this work we investigate a one-dimensional cloud of spinless fermions loaded into an optical cavity and pumped by a pair of transverse laser beams of unequal intensities. We found superradiant steady states which did not appear in the bosonic case in the nondissipative limit. In the dissipative case, we found a bistable regime, in which two superradiant phases coexist. When increasing the dissipation, a self-organized dynamically unstable phase appears and suppresses the bistable regime. Based on these superradiant phases and hysteresis in the bistable regime, we design a unidirectional topological pumping. Unlike the usual topological pumping in which the driving protocol breaks time-reversal symmetry, the driving protocol can be time-reversal invariant in our proposal. It is the self-organization and dissipation that stabilize the quantization of the pumping. Our work provides insights into the behavior of fermions in cavity systems and paves the way for future studies of topological phenomena inside cavities.

The rest of this paper is organized as follows. We first show our setup and derive a tight-binding model. Then we investigate the nondissipative case, mainly studying the phase transitions. Further, we turn on the dissipation, and see how the phases and transitions are changed by dissipation. Last, we propose a unidirectional topological pumping by making use of the transition structure.

II. THE SETUP AND MODEL

The physical setup is shown in Fig. 1, where fermionic atoms are loaded into a single-mode optical cavity, which is set along the y axis. The electrical field of the cavity mode is $\hat{\mathbf{E}}_c(\mathbf{r}) = \xi(\hat{a} + \hat{a}^\dagger) \cos(k_c y) \mathbf{e}_z$, where ξ is the electric field strength of a single photon, and \hat{a} (\hat{a}^\dagger) is the

*zw8796@ustc.edu.cn

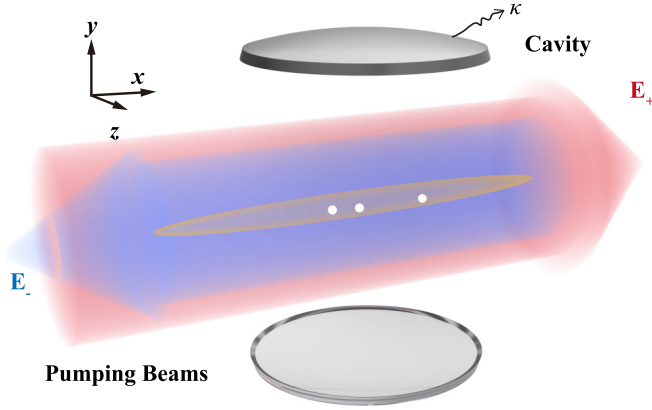


FIG. 1. Schematic illustration of spinless fermionic atoms trapped in a cavity coupled with imbalanced transverse pumping beams. The fermion atoms are restricted in a 1D tube along the pumping beams.

annihilating (creating) operator of the cavity photons. The atomic cloud is illuminated by a pair of counterpropagating pumping lasers along the x axis. The electronic field of the pumping beams is $\mathbf{E}(\mathbf{r}, t) = \mathbf{E}_+(\mathbf{r}, t) + \mathbf{E}_-(\mathbf{r}, t)$, with counterpropagating plane waves $\mathbf{E}_\pm(\mathbf{r}, t) = E_\pm \cos(\pm k_p x - \omega_p t) \mathbf{e}_z$, where k_p is the wave vector of the pumping beam with frequency ω_p .

In such a setup, atoms feel a cavity-dependent potential,

$$V(\mathbf{r}) = V_{\text{pump}}(\mathbf{r}) + V_{\text{cavity}}(\mathbf{r}) + V_{\text{inter}}(\mathbf{r}). \quad (1)$$

Here $V_{\text{pump}}(\mathbf{r}) = V_p \cos^2(k_p x)$ is the lattice generated by the pumping lasers, and $V_p = u_s E_+ E_-$ is the corresponding lattice depth. $V_{\text{cavity}}(\mathbf{r}) = V_c \cos^2(k_c y) \hat{a}^\dagger \hat{a}$ is the lattice generated by the cavity field, and $V_c = u_s \xi^2$ is the ac Stark shift induced by one cavity photon, and u_s is the scalar polarizability of the atoms. The interference between the pumping beams and cavity field generates the following lattice:

$$V_{\text{inter}}(\mathbf{r}) = V_R \cos(k_p x) \cos(k_c y) (\hat{a} + \hat{a}^\dagger)/2 \\ + V_I \sin(k_p x) \cos(k_c y) (\hat{a} - \hat{a}^\dagger)/2i,$$

where $V_R = u_s \xi (E_+ + E_-)$ and $V_I = u_s \xi (E_+ - E_-)$. It describes the process of scattering a photon by atoms from pumping lasers into the cavity and vice versa. In this work we consider only blue atomic detuning, such that $u_s > 0$. Note that in the case of balanced pumping, $E_+ = E_-$, thus $V_I = 0$, and atoms are coupled only to the real quadrature of the cavity. When the pumping is imbalanced $E_+ \neq E_-$, $V_I \neq 0$, and atoms are coupled to both real and imaginary quadratures.

In this work we further consider the motion of atoms to be restricted along the direction of the pumping beams [43]. This can be achieved by additionally applying two pairs of far-detuned strong trapping lasers from $\mathbf{e}_y + \mathbf{e}_z$ and $\mathbf{e}_y - \mathbf{e}_z$ directions, such that the atoms can move only along the x direction. Therefore, the system is effectively one-dimensional, and the corresponding second quantized

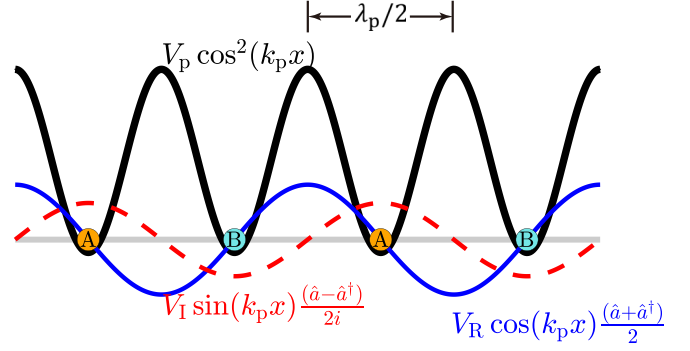


FIG. 2. Lattice potentials in the continuum. We obtain the tight binding model by considering only the s -band Wannier basis with the nearest hopping.

Hamiltonian is given by

$$\hat{H} = -\Delta_c \hat{a}^\dagger \hat{a} + \int dx \hat{\psi}^\dagger(x) \left[\frac{-\nabla^2}{2m} + V_p \cos^2(k_p x) \right] \hat{\psi}(x), \\ + \int dx \hat{\psi}^\dagger(x) [V_R \cos(k_p x) (\hat{a} + \hat{a}^\dagger)/2] \hat{\psi}(x) \\ + \int dx \hat{\psi}^\dagger(x) [V_I \sin(k_p x) (\hat{a} - \hat{a}^\dagger)/2i] \hat{\psi}(x), \quad (2)$$

where $\hat{\psi}(x)$ is the field operator of fermions. $\Delta_c = \omega_p - \omega_c - NV_c$ is the effective cavity detuning, and N is the total number of fermions.

In the strong pumping regime, the lattice generated by the pumping lasers is so deep, such that we can apply the tight-binding approximation. As shown in Fig. 2, the unit cell of the pumping lattice is enlarged due to the double period of the interference lattice. We denote the two s orbits in one unit cell as A and B, and obtain the tight-binding Hamiltonian as

$$\hat{H}_{\text{TB}} = -\Delta_c \hat{a}^\dagger \hat{a} + \sum_j J_0 (\hat{c}_{j,B}^\dagger \hat{c}_{j,A} + \hat{c}_{j+1,A}^\dagger \hat{c}_{j,B} + \text{H.c.}) \\ + \sum_j J_1 \frac{(\hat{a} + \hat{a}^\dagger)}{2} (-\hat{c}_{j,B}^\dagger \hat{c}_{j,A} + \hat{c}_{j+1,A}^\dagger \hat{c}_{j,B} + \text{H.c.}) \\ + \sum_j J_2 \frac{(\hat{a} - \hat{a}^\dagger)}{2i} (\hat{c}_{j,A}^\dagger \hat{c}_{j,A} - \hat{c}_{j,B}^\dagger \hat{c}_{j,B}), \quad (3)$$

where

$$J_0 = \int_x w^* \left(x - \frac{\lambda_p}{4} \right) \left[\frac{-\nabla^2}{2m} + V_p \cos^2(k_p x) \right] w \left(x + \frac{\lambda_p}{4} \right), \\ J_1 = V_R \int_x w^* \left(x - \frac{\lambda_p}{4} \right) \cos(k_p x) w \left(x + \frac{\lambda_p}{4} \right), \\ J_2 = V_I \int_x w^* \left(x - \frac{\lambda_p}{4} \right) \sin(k_p x) w \left(x - \frac{\lambda_p}{4} \right).$$

Here $w(x)$ is the s -band Wannier wave function of the pumping lattice. Note that this model is a cavity-dependent Rice-Mele model. The real quadrature of the cavity, $(\hat{a} + \hat{a}^\dagger)/2$, will tune the hopping ratio between intra- and interunit cells, while the imaginary quadrature of the cavity, $(\hat{a} - \hat{a}^\dagger)/2i$, will change the onsite energy of A and B

sublattices. In the momentum space, the Hamiltonian can be expressed as

$$\hat{H}_{\text{TB}} = -\Delta_c \hat{a}^\dagger \hat{a} + \sum_k \hat{\Psi}_k^\dagger [\mathbf{B}_k(\hat{a}, \hat{a}^\dagger) \cdot \boldsymbol{\sigma}] \hat{\Psi}_k, \quad (4)$$

where $\hat{\Psi}_k = (\hat{c}_{k,A}, \hat{c}_{k,B})^T$, $\boldsymbol{\sigma}$ is the Pauli matrix vector, and the momentum-dependent effective magnetic field is

$$\mathbf{B}_k(\hat{a}, \hat{a}^\dagger) = \begin{pmatrix} J_0(1 + \cos k) + J_1(\hat{a} + \hat{a}^\dagger)(-1 + \cos k)/2 \\ [J_0 + J_1(\hat{a} + \hat{a}^\dagger)/2] \sin k \\ J_2(\hat{a} - \hat{a}^\dagger)/2i \end{pmatrix}. \quad (5)$$

Besides the coherent process governed by the Hamiltonian, the leaking of photons from the cavity leads to dissipative dynamics. The evolution can be described by a Lindblad quantum master equation

$$\partial_t \hat{\rho} = -i[\hat{H}_{\text{TB}}, \hat{\rho}] + \kappa(2\hat{a}\hat{\rho}\hat{a}^\dagger - \{\hat{a}^\dagger\hat{a}, \hat{\rho}\}), \quad (6)$$

where κ is the photon loss rate.

In the following, we apply the mean-field approximation to investigate the dynamics of this atom-cavity system. The mean-field approximation ignores the quantum fluctuations. It is valid only in the regime where fluctuations are much smaller than the mean values. In the superradiant phases, the cavity field is macroscopically occupied. Thus, the fluctuation of the cavity field is on the order of $O(1)$, which is much smaller than the mean value with the order of $O(\sqrt{N})$, where N is the total number of the atoms. Thus, the mean-field approximation can be applied in the superradiant regime. However, near critical points, the fluctuations will dominate, and the mean-field approximation cannot be trusted.

We define the mean cavity field as $\alpha(t) = \langle \hat{a}(t) \rangle$, and $\mathbf{m}_k(t) = \langle \hat{\Psi}_k^\dagger(t) \boldsymbol{\sigma} \hat{\Psi}_k(t) \rangle$, which can be regarded as mean pseudospins of fermions in the momentum space. The mean-field self-consistent equations of motion of $\alpha(t)$ and $\mathbf{m}_k(t)$ are given by

$$i\partial_t \alpha = (-\Delta_c - i\kappa)\alpha + \sum_k \boldsymbol{\Theta}_k \cdot \mathbf{m}_k, \quad (7)$$

$$\partial_t \mathbf{m}_k = 2\mathbf{B}_k(\alpha, \alpha^*) \times \mathbf{m}_k, \quad (8)$$

where

$$\boldsymbol{\Theta}_k = \frac{\partial \mathbf{B}_k(\alpha, \alpha^*)}{\partial \alpha^*} = \frac{1}{2} \begin{pmatrix} J_1(-1 + \cos k) \\ J_1 \sin k \\ iJ_2 \end{pmatrix}. \quad (9)$$

We numerically solved the coupled equations of motion (7) and (8), starting from the equilibrium initial state with $\langle \hat{\Psi}_k^\dagger(0) \hat{\Psi}_k(0) \rangle = \theta(k_f - |k|)$, where the $\theta(k_f - |k|)$ is the Heaviside step function representing Fermi distribution, and k_f is the Fermi momentum determined by total number of fermions N . Then one can obtain the dynamics of the cavity field and fermions.

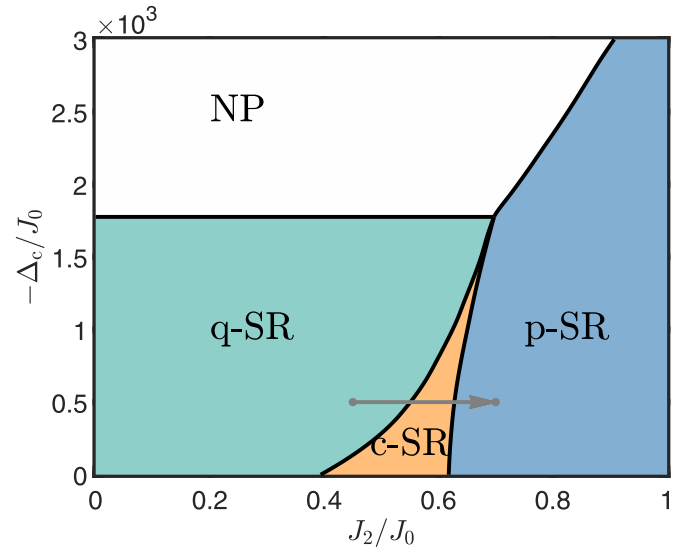


FIG. 3. Phase diagram without dissipation with $J_1/J_0 = 0.5$, filling $\nu = 0.4$. There are one normal phase (NP) and three superradiant (SR) phases. Four phases meet at a quadra-critical point. The gray path will be mentioned in Fig. 5.

III. NONDISSIPATIVE CASE

In this section we will first explore this atom-cavity model in the nondissipative case $\kappa = 0$. This will pave the way to the dissipative case.

By solving the mean-field equation of motions, we obtain the resulting ground-state phase diagram of fixed J_1 shown in Fig. 3. The diagram includes one normal phase (NP) with $\alpha = 0$ and three distinct superradiant (SR) phases $\alpha \neq 0$. When the photon detuning $|\Delta_c|$ is sufficiently large, the system is in the normal phase. In the regime of small $|\Delta_c|$ and small J_2 , the system is in the q-SR phase, which stands for a superradiant phase where the cavity field α is real. When J_2 dominates, the system enters the p-SR phase, where α is purely imaginary. Between them there is a c-SR phase where the phase of the cavity field is not fixed and can be tuned continuously. The four phases meet at a quadra-critical point.

The symmetry group of the Hamiltonian is product of two \mathbb{Z}_2 groups, $\{\mathcal{I}, \mathcal{T}_R\} \otimes \{\mathcal{I}, \mathcal{T}_I\} = \{\mathcal{I}, \mathcal{T}_R, \mathcal{T}_I, \mathcal{U}\}$ [44], where

$$\begin{aligned} \mathcal{T}_R &: \begin{cases} \hat{a} \rightarrow \hat{a}^\dagger \\ x \rightarrow -x \end{cases}, \\ \mathcal{T}_I &: \begin{cases} \hat{a} \rightarrow -\hat{a}^\dagger \\ x \rightarrow -x + \lambda_p/2 \end{cases}, \\ \mathcal{U} &: \begin{cases} \hat{a} \rightarrow -\hat{a} \\ x \rightarrow x + \lambda_p/2 \end{cases}. \end{aligned}$$

Note that \mathcal{T}_R represents a real-axis reflection of cavity field on the complex plane, combining with the spatial reflection of fermions. \mathcal{T}_I represents an imaginary-axis reflection with spatial reflection plus spatial translation of fermions. $\mathcal{U} = \mathcal{T}_R \otimes \mathcal{T}_I$ is a π rotation of the cavity field combining a spatial translation of fermions.

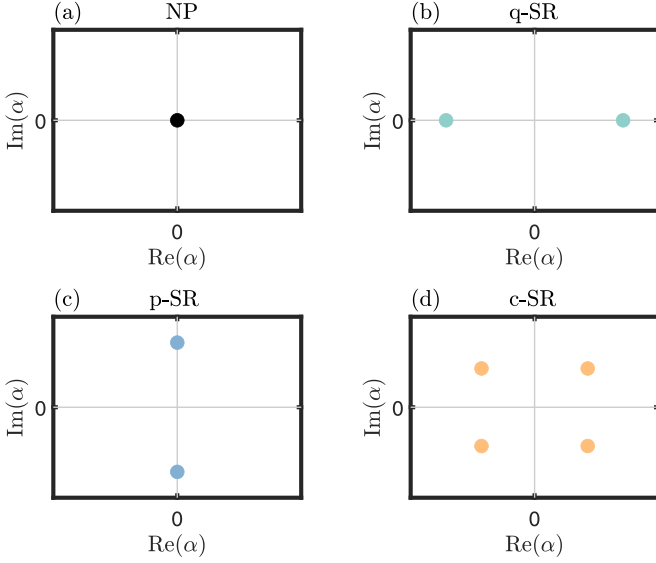


FIG. 4. Schematic configurations of α of the ground states on the complex plane in four phases. NP: $\alpha = 0$; q-SR: Two opposite real numbers; p-SR: Two opposite imaginary numbers; c-SR: Four numbers in four quadrants.

We show configurations of the cavity field in different phases in Fig. 4 and their symmetries in Table I. All symmetries are maintained in the NP. In SR phases, including q-SR, p-SR and c-SR phases, the \mathcal{U} symmetry is broken, but the \mathcal{T}_R or \mathcal{T}_I symmetry may survive respectively. The q-SR phase breaks the \mathcal{T}_I symmetry and keeps the \mathcal{T}_R symmetry, thus the phase of cavity is either 0 or π . The p-SR phase is invariant under \mathcal{T}_I but breaks the \mathcal{T}_R symmetry. So the cavity phase is either $\pi/2$ or $-\pi/2$. The c-SR phase breaks \mathcal{T}_R , \mathcal{T}_I , and \mathcal{U} symmetries, therefore its cavity phase can be tuned continuously.

Next, we investigate the transitions between these phases. We observe that the transitions are second-order. Starting from NP, by decreasing the $|\Delta_c/J_0|$, the system will enter the q-SR phase. The \mathcal{T}_I symmetry is broken spontaneously as two energy minimums emerge from $\alpha = 0$ and then divide oppositely on the real axis, but the \mathcal{T}_R symmetry is preserved. As moving further into the c-SR phase, the \mathcal{T}_R symmetry is broken by increasing J_2 , and each minimum is split into a complex conjugate pair. In the c-SR phase, the order parameter α changes continuously in four quadrants. Approaching the transition between the c-SR and p-SR, the upper or lower pair coalesces into a purely imaginary one, respectively, and the \mathcal{T}_I symmetry is restored. Finally, the system recovers the

TABLE I. Comparison table of symmetries in different phases.

Phase	$\arg(\alpha)$	\mathcal{T}_R	\mathcal{T}_I	\mathcal{U}
NP	—	✓	✓	✓
q-SR	$0, \pi$	✓	×	×
p-SR	$\pm\pi/2$	×	✓	×
c-SR	Arbitrary	×	×	×

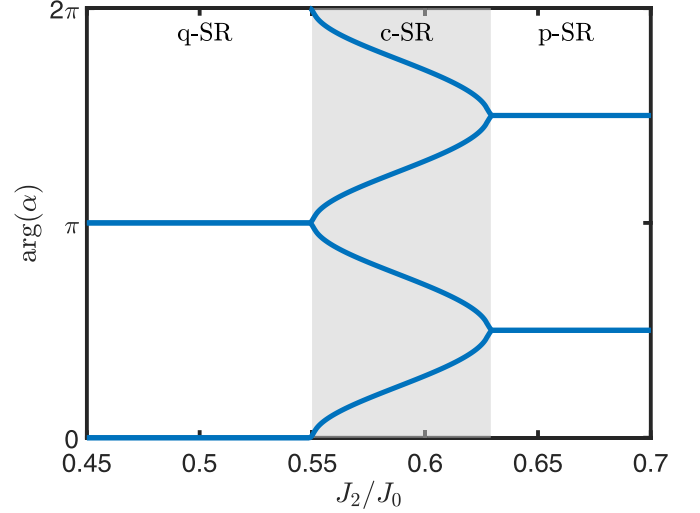


FIG. 5. The phase of α changes along the gray path in Fig. 3 across the c-SR phases. In the q-SR/p-SR phase, there are two steady states whose phases are locked to $(0, \pi) \pm \frac{\pi}{2}$. In the c-SR phase, the remaining symmetry is broken, degeneracy is doubled. The transitions are all continuous.

\mathcal{T}_R symmetry by the merging of the imaginary pairs at the transition to the NP. Figure 5 shows how the phases of the cavity field change continuously along the path depicted in Fig. 3.

IV. DISSIPATIVE CASE

In this section we will consider the fate of these phases in the presence of dissipation, $\kappa \neq 0$. In this situation we numerically solve the equations of motion and consider its long-time dynamics to seek the steady states. The phase diagram in the presence of dissipation is plotted in Fig. 6. In the small κ regime, there exist five different regimes: A steady NP and two steady SR phases, which we denote as SR-I and SR-II. The SR-I phase is reminiscent of the q-SR phase. However, the phase of the cavity is not locked at 0 and π ; instead it has a phase shift $\phi_\kappa = \tan^{-1}(\frac{\kappa}{\Delta_c})$ relative to the q-SR phase. Similarly, the SR-II phase is reminiscent of the p-SR phase, but also with a phase shift ϕ_κ . In the limit $\kappa \rightarrow 0$, the SR-I and SR-II phases will continuously cross over to the q-SR and p-SR phases; see Fig. 7. From the symmetry point of view, we note that both the \mathcal{T}_R and \mathcal{T}_I symmetries are absent in the presence of dissipation. This can be seen from the Lindblad quantum master equation. The only symmetry that survives in the presence of dissipation is the \mathcal{U} symmetry. Thus, there are no q-SR and p-SR phases in the dissipative case. Between the SR-I and SR-II phases, there is a bistable regime, in which both the SR-I and SR-II phases are the steady state of the system. Whether the system stays in the SR-I or SR-II state depends on the initial condition. This bistable regime is reminiscent of the c-SR phase in the nondissipative limit. When $|\Delta_c|$ is small, there is an unstable phase, which does not exist in the nondissipative case. In this phase, the system will not reach a steady state. The dissipation will drive both the cavity field and fermions to evolve incessantly. The unstable phase

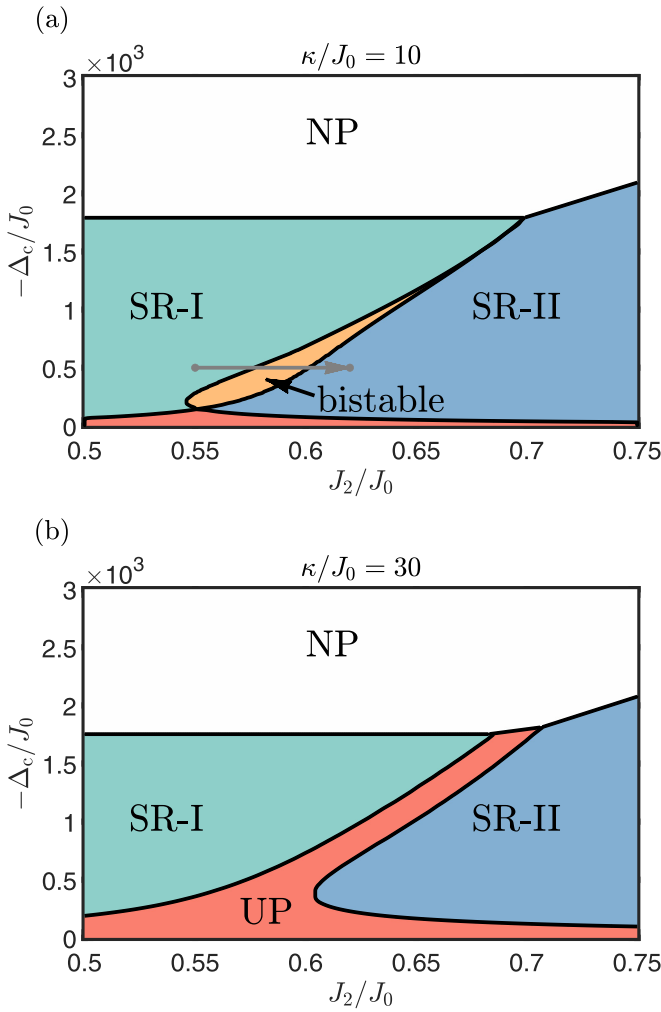


FIG. 6. The dissipative phase diagram under small and large dissipation, respectively, with parameters $J_1/J_0 = 0.5$, $\nu = 0.4$. The red region represents the unstable phase. It gradually replaces the bistable regime as κ increases. The gray path will be mentioned in Fig. 9.

has already been observed in bosonic gases coupled with an imbalanced pumped cavity. In the bosonic case, since there is no c-SR phase or bistable regime, the unstable phase emerges directly from the first-order transition between the two super-radiant phases as $\kappa > 0$ [41,42]. Here with fermions inside an imbalanced pumped cavity, as κ increases, we observe that the unstable phase gradually squeezes the bistable regime, eventually replacing it when κ becomes sufficiently large; see Fig. 8.

Phase transitions are also strongly influenced by dissipation. In contrast with the second-order transition in the nondissipative case, α now switches discontinuously when across the bistable regime and exhibits a hysteresis structure; see Fig. 9. When we ramp J_2 up slowly from the SR-I, the system will move continuously into the bistable regime, and will suddenly jump to the SR-II phase at the right boundary. Conversely, if the system is initially prepared in the SR-II phase, then the jump will take place on the left boundary when J_2 is ramped down.

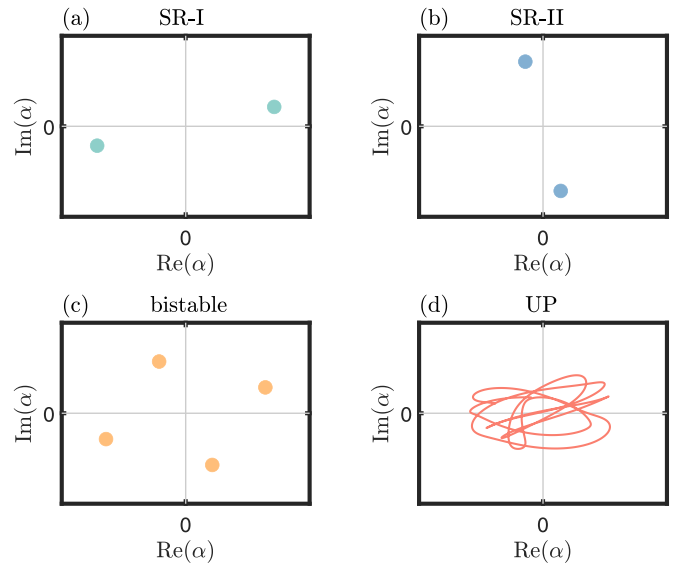


FIG. 7. Schematic configurations of α of the steady states on the complex plane in SR phases, and the last panel demonstrates the trajectory of evolution in the unstable phase.

V. DISSIPATION-INDUCED UNIDIRECTIONAL TOPOLOGICAL PUMPING

It has been shown by Thouless that when parameters of a 1D insulator are driven adiabatically to complete a cycle, the charge pumped through the bulk is quantized [24,45,46]. To pump nonzero quantized charges, the way of the external driving has to break the time-reversal symmetry (TRS). Here, on the contrary, we employ the hysteresis structure of these superradiance states to realize a unidirectional topological pumping by a TRS-preserving driving protocol. It should be noted that while talking about topological pumping, the system is supposed to be an insulator. Thus in our system,

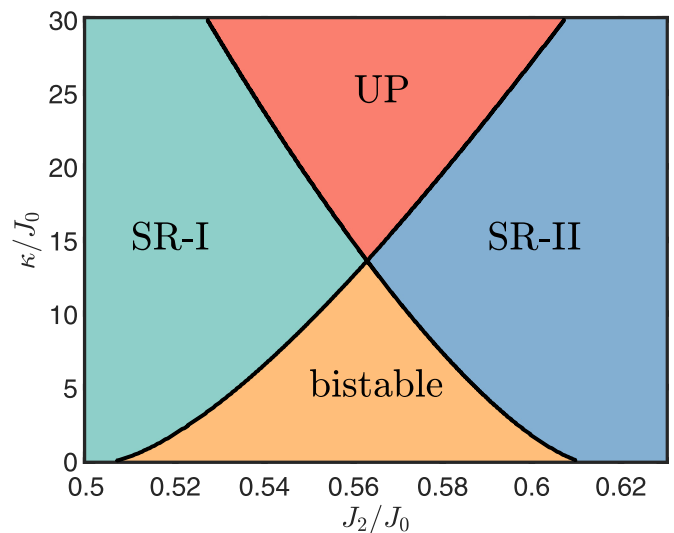


FIG. 8. A cross section of the former phase diagrams with fixed $\Delta_c = -300J_0$ but different κ . The dissipation first reduces the width of the bistable regime to zero and then brings about an unstable phase.

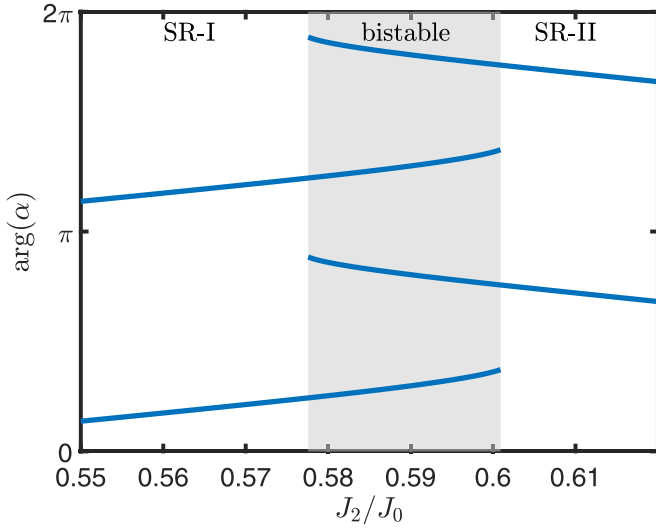


FIG. 9. The phase of α changes along the gray path in Fig. 6 across the bistable regime. The continuous phase transitions turn into a hysteresis.

fermions should be at half filling. Phase diagrams at half filling are shown in the Appendix; the SR phases and the transition structures of the cavity field are similar while the NP disappears.

We perform the adiabatic driving $J_2(t) = \bar{J}_2 + \delta J_2 \cos(\Omega t)$ with fixed Δ_c , where $\Omega = 2\pi/T$, and T is the period of driving. Such a driving protocol preserves the TRS. The numerical results are presented in Fig. 10. Our simulations reveal that the evolution of the cavity field $\alpha(t)$ forms a full circle enclosing the origin on the complex plane within a doubled period $2T$. That indicates this driven system exhibits

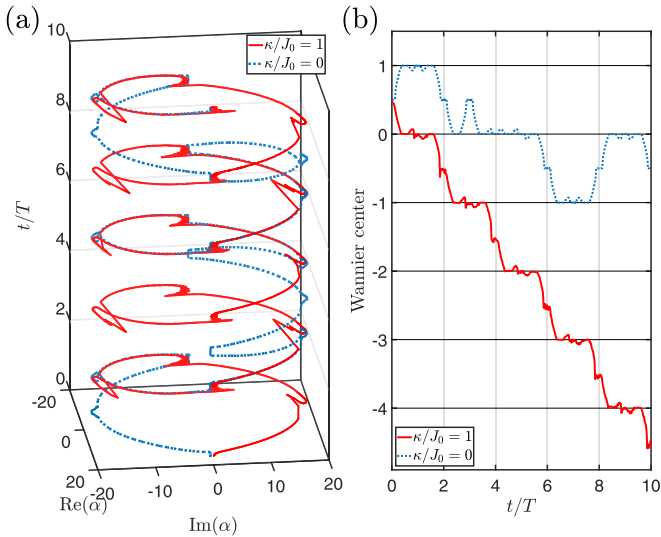


FIG. 10. The numerical results of time evolution in topological pumping, where $J_2/J_0 = 0.625 - 0.125 \cos(\frac{2\pi}{T}t)$ with the period $T = 2000\pi/J_0$. (a) The trajectory of α on the complex plane, it forms a circle around the origin and has four discontinuous jumps across the axes. The Wannier center flow in (b) manifests the topological pumping obviously.

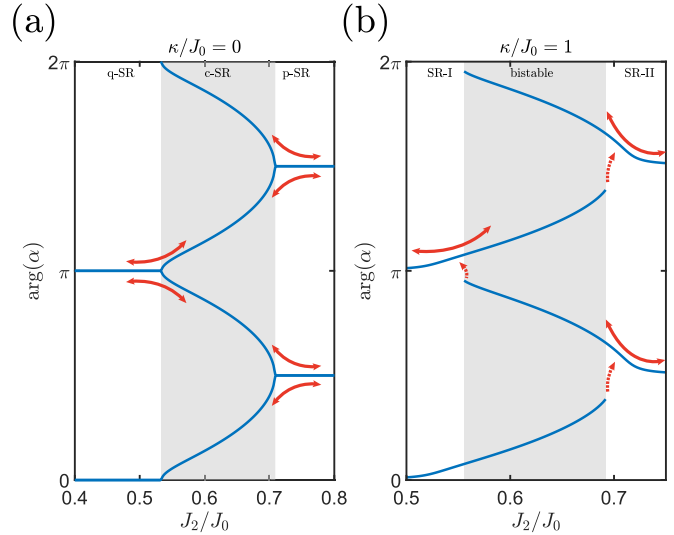


FIG. 11. The phase of α across the c-SR phase or bistable regime in the (a) nondissipative and (b) dissipative case, whose structure looks like a ladder. The dissipation can turn the bidirectional ladder into a unidirectional one.

a discrete time crystalline order. As the atomic band can be mapped to a cavity-dependent Rice-Mele model, we then observe a quantized pumping in the Wannier center trajectory through time evolution [47]; see Fig. 10(b).

The physical process under driving is interpreted as the red arrows in Fig. 11(b). Starting the driving from the SR-I phase, the cavity phase is close to 0, and when adiabatically increasing J_2 , the system will self-organized follow the driving to enter the bistable regime smoothly and stay at one of the instantaneous stable states. When J_2 reaches the right boundary of the bistable regime, the bistability vanishes, and the system is forced to jump to the SR-II phase. The excitation energy in this jump process can be dissipated by the loss of cavity photons, and the system will catch the closer one of the two SR-II steady states in a short time. In this regime, the system will again self-organized follow the driving, and the cavity phase is driven close to $\pi/2$. After half a period, J_2 will decrease, and the system will again enter the bistable regime adiabatically, staying at an alternative stable state. When J_2 is small, the system will jump to an SR-I state with the cavity phase α close to π . Repeat the driving for another period, and the cavity field will go back to form a cycle on the complex plane. In this process, one particle is pumped through the bulk.

We also simulate the same driving protocol without dissipation, i.e., $\kappa = 0$. The results are shown in Fig. 10. Note that driving the parameter adiabatically between the q-SR and p-SR phases causes the cavity field α to change slowly, resulting in a quantized displacement of the Wannier center during the evolution. However, the direction of the displacement is not controllable due to the spontaneous symmetry breaking at the transitions to the c-SR phase, as shown as red arrows in Fig. 11(a). At the phase boundaries, the phase of α may increase or may decrease, leading to a random back-and-forth displacement of the Wannier center over long timescales. For a long-time average, the mean displacement is zero.

Compared to the nondissipative case, we conclude that the dissipation plays a dual role. First, the presence of dissipation changes the continuous phase transitions into a bistable hysteresis structure, preventing charge pumping in both directions. Second, it attracts the system towards a closer steady state while losing stability, which contributes to the unidirectional motion. It should be emphasized that this direction of the pumping cannot be reversed by reversing the driving cycle since the driving protocol itself preserves the TRS. The key here is that the protocol does not change the topology of the band directly like in other ordinary pumping systems. This band is self-organized as $\alpha(t)$ is not manually controlled. Then, with the help of dissipation, this TRS-preserving protocol leads to a counterrotating $\alpha(t)$ on the complex plane, which breaks the TRS. As a result, the cavity-dependent band generates the topological pumping.

VI. SUMMARY

In summary, we have investigated the behavior of spinless fermions loaded into an optical cavity, which is pumped by transverse beams of unequal intensities. Multiple superradiant phases and a dynamical phase are found. Based on the hysteresis structure of superradiant phases, we predict the phenomenon of unidirectional topological pumping, in which the dissipation plays an important role. Our prediction can be observed in current experiments. Future research could be addressed in following directions. First, our proposal could be generalized to a higher dimension, where the nonequilibrium phases of fermions with imbalanced pumping have not been explored. Second, loading the spinful fermions into the cavity, the direct interaction between fermions should be considered. The interplay between the superradiance, strong correlations, and dissipation could induce unexpected phenomena. In this situation, one should go beyond the mean-field approximation.

ACKNOWLEDGMENT

This research is supported by the Innovation Program for Quantum Science and Technology (Grant No. 2021ZD0302000).

APPENDIX: PHASE DIAGRAMS AT HALF FILLING

While talking about topology in Sec. V, the band actually should be half-filled. We show more details about this situation in this Appendix.

At half filling, the Fermi surface nesting arises due to the interference lattice coupling the two Fermi momenta $\pm k_f$ [16–18]. Thus, the total energy will be lowered by an infinitesimal α , leading to the disappearance of the NP. This is also observed when $\kappa > 0$. The phase diagrams are depicted in Fig. 12. It is noteworthy that though the c-SR phase and the bistable regime become narrower as $|\Delta_c|$ increases, they will never disappear.

In the nondissipative q-SR phase, where α is real, the mean-field Hamiltonian can be simplified to a

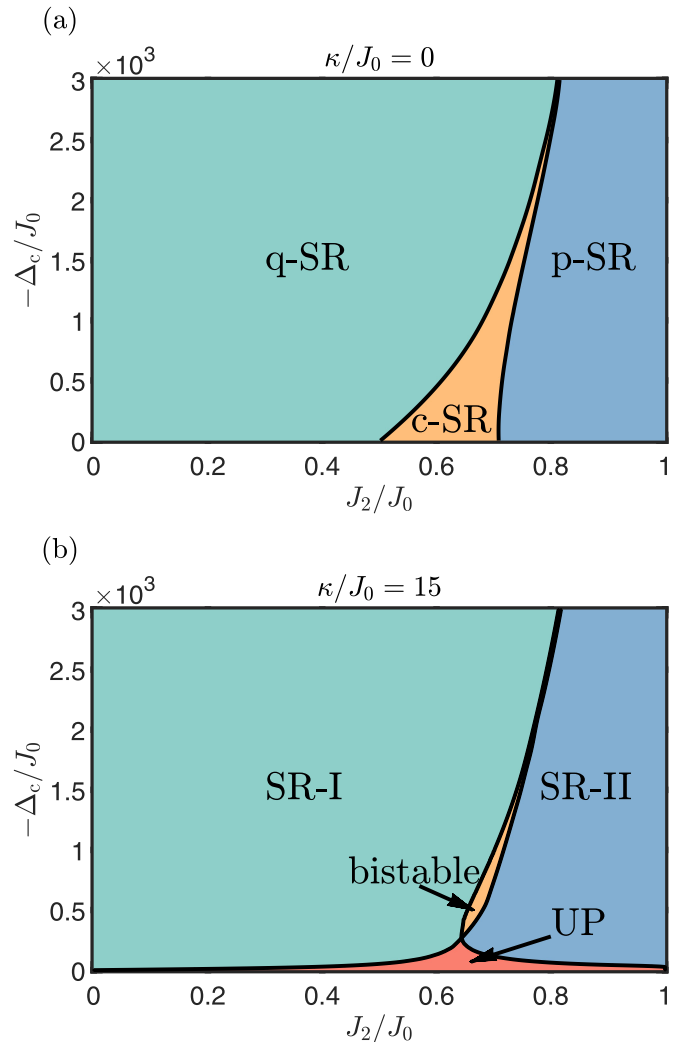


FIG. 12. Phase diagrams when half filling $\nu = 0.5$. The NP is unfavored due to the Fermi surface nesting.

Su-Schrieffer-Heeger (SSH) model [22],

$$\mathbf{B}_k(\alpha, \alpha^*) = \begin{pmatrix} J_0(1 + \cos k) + J_1\alpha(-1 + \cos k) \\ (J_0 + J_1\alpha) \sin k \\ 0 \end{pmatrix}. \quad (\text{A1})$$

The SSH model has two topologically distinct phases characterized by the quantized Wannier center [48–50],

$$w = \frac{1}{2\pi} \int_{BZ} dk \langle \psi_k | i \frac{\partial}{\partial k} | \psi_k \rangle, \quad (\text{A2})$$

which can either be 0 or 0.5. When $\alpha > 0$, the intercell hopping ($J_0 + J_1\alpha$) is larger than the intracell hopping ($J_0 - J_1\alpha$) resulting in a topologically nontrivial phase with $w = 0.5$. This indicates the presence of a finite dipole momentum in the bulk, along with a pair of zero-energy edge states at the boundaries. On the other hand, when $\alpha < 0$, the bulk dipole momentum vanishes $w = 0$, and no edge state exists. Therefore, the symmetry in the q-SR phase is spontaneously broken, leading to either a topological nontrivial or a trivial phase, depending on the sign of α .

- [1] R. H. Dicke, Coherence in spontaneous radiation processes, *Phys. Rev.* **93**, 99 (1954).
- [2] Y. K. Wang and F. T. Hioe, Phase transition in the Dicke model of superradiance, *Phys. Rev. A* **7**, 831 (1973).
- [3] K. Hepp and E. H. Lieb, On the superradiant phase transition for molecules in a quantized radiation field: The Dicke maser model, *Ann. Phys.* **76**, 360 (1973).
- [4] P. Domokos and H. Ritsch, Collective cooling and self-organization of atoms in a cavity, *Phys. Rev. Lett.* **89**, 253003 (2002).
- [5] J. K. Asbóth, P. Domokos, H. Ritsch, and A. Vukics, Self-organization of atoms in a cavity field: Threshold, bistability, and scaling laws, *Phys. Rev. A* **72**, 053417 (2005).
- [6] F. Dimer, B. Estienne, A. S. Parkins, and H. J. Carmichael, Proposed realization of the Dicke-model quantum phase transition in an optical cavity QED system, *Phys. Rev. A* **75**, 013804 (2007).
- [7] D. Nagy, G. Szirmai, and P. Domokos, Self-organization of a Bose-Einstein condensate in an optical cavity, *Eur. Phys. J. D* **48**, 127 (2008).
- [8] E. G. Dalla Torre, S. Diehl, M. D. Lukin, S. Sachdev, and P. Strack, Keldysh approach for nonequilibrium phase transitions in quantum optics: Beyond the Dicke model in optical cavities, *Phys. Rev. A* **87**, 023831 (2013).
- [9] A. Baksic and C. Ciuti, Controlling discrete and continuous symmetries in “superradiant” phase transitions with circuit QED systems, *Phys. Rev. Lett.* **112**, 173601 (2014).
- [10] L. M. Sieberer, M. Buchhold, and S. Diehl, Keldysh field theory for driven open quantum systems, *Rep. Prog. Phys.* **79**, 096001 (2016).
- [11] J. Larson and E. K. Irish, Some remarks on ‘superradiant’ phase transitions in light-matter systems, *J. Phys. A: Math. Theor.* **50**, 174002 (2017).
- [12] M. Soriente, T. Donner, R. Chitra, and O. Zilberberg, Dissipation-induced anomalous multicritical phenomena, *Phys. Rev. Lett.* **120**, 183603 (2018).
- [13] J. Fan, G. Chen, and S. Jia, Atomic self-organization emerging from tunable quadrature coupling, *Phys. Rev. A* **101**, 063627 (2020).
- [14] K. Baumann, C. Guerlin, F. Brennecke, and T. Esslinger, Dicke quantum phase transition with a superfluid gas in an optical cavity, *Nature (London)* **464**, 1301 (2010).
- [15] J. Klinder, H. Keßler, M. Wolke, L. Mathey, and A. Hemmerich, Dynamical phase transition in the open Dicke model, *Proc. Natl. Acad. Sci. USA* **112**, 3290 (2015).
- [16] Y. Chen, Z. Yu, and H. Zhai, Superradiance of degenerate Fermi gases in a cavity, *Phys. Rev. Lett.* **112**, 143004 (2014).
- [17] J. Keeling, M. J. Bhaseen, and B. D. Simons, Fermionic superradiance in a transversely pumped optical cavity, *Phys. Rev. Lett.* **112**, 143002 (2014).
- [18] F. Piazza and P. Strack, Umklapp superradiance with a collisionless quantum degenerate Fermi gas, *Phys. Rev. Lett.* **112**, 143003 (2014).
- [19] Y. Chen, H. Zhai, and Z. Yu, Superradiant phase transition of Fermi gases in a cavity across a Feshbach resonance, *Phys. Rev. A* **91**, 021602(R) (2015).
- [20] C. Kollath, A. Sheikhan, S. Wolff, and F. Brennecke, Ultracold fermions in a cavity-induced artificial magnetic field, *Phys. Rev. Lett.* **116**, 060401 (2016).
- [21] A. Sheikhan, F. Brennecke, and C. Kollath, Cavity-induced generation of nontrivial topological states in a two-dimensional Fermi gas, *Phys. Rev. A* **94**, 061603(R) (2016).
- [22] F. Mivehvar, H. Ritsch, and F. Piazza, Superradiant topological Peierls insulator inside an optical cavity, *Phys. Rev. Lett.* **118**, 073602 (2017).
- [23] D. Yu, J.-S. Pan, X.-J. Liu, W. Zhang, and W. Yi, Topological superradiant state in Fermi gases with cavity induced spin-orbit coupling, *Front. Phys.* **13**, 136701 (2018).
- [24] E. Colella, S. Ostermann, W. Niedenzu, F. Mivehvar, and H. Ritsch, Antiferromagnetic self-ordering of a Fermi gas in a ring cavity, *New J. Phys.* **21**, 043019 (2019).
- [25] X. Zhang, Y. Chen, Z. Wu, J. Wang, J. Fan, S. Deng, and H. Wu, Observation of a superradiant quantum phase transition in an intracavity degenerate Fermi gas, *Science* **373**, 1359 (2021).
- [26] V. Helsen, T. Zwettler, F. Mivehvar, E. Colella, K. Roux, H. Konishi, H. Ritsch, and J.-P. Brantut, Density-wave ordering in a unitary Fermi gas with photon-mediated interactions, *Nature (London)* **618**, 716 (2023).
- [27] M. J. Bhaseen, J. Mayoh, B. D. Simons, and J. Keeling, Dynamics of nonequilibrium Dicke models, *Phys. Rev. A* **85**, 013817 (2012).
- [28] F. Piazza and H. Ritsch, Self-ordered limit cycles, chaos, and phase slippage with a superfluid inside an optical resonator, *Phys. Rev. Lett.* **115**, 163601 (2015).
- [29] W. Zheng and N. R. Cooper, Superradiance induced particle flow via dynamical gauge coupling, *Phys. Rev. Lett.* **117**, 175302 (2016).
- [30] P. Kirton and J. Keeling, Superradiant and lasing states in driven-dissipative Dicke models, *New J. Phys.* **20**, 015009 (2018).
- [31] H. Keßler, J. G. Cosme, M. Hemmerling, L. Mathey, and A. Hemmerich, Emergent limit cycles and time crystal dynamics in an atom-cavity system, *Phys. Rev. A* **99**, 053605 (2019).
- [32] E. I. Rodríguez Chiacchio and A. Nunnenkamp, Dissipation-induced instabilities of a spinor Bose-Einstein condensate inside an optical cavity, *Phys. Rev. Lett.* **122**, 193605 (2019).
- [33] B. Buča and D. Jaksch, Dissipation induced nonstationarity in a quantum gas, *Phys. Rev. Lett.* **123**, 260401 (2019).
- [34] R. J. L. Tuquero, J. Skulte, L. Mathey, and J. G. Cosme, Dissipative time crystal in an atom-cavity system: Influence of trap and competing interactions, *Phys. Rev. A* **105**, 043311 (2022).
- [35] E. Colella, A. Kosior, F. Mivehvar, and H. Ritsch, Open quantum system simulation of Faraday’s induction law via dynamical instabilities, *Phys. Rev. Lett.* **128**, 070603 (2022).
- [36] A. Kosior, H. Ritsch, and F. Mivehvar, Nonequilibrium phases of ultracold bosons with cavity-induced dynamic gauge fields, *SciPost Phys.* **15**, 046 (2023).
- [37] X. Nie and W. Zheng, Mode softening in time-crystalline transitions of open quantum systems, *Phys. Rev. A* **107**, 033311 (2023).
- [38] P. Zupancic, D. Dreon, X. Li, A. Baumgärtner, A. Morales, W. Zheng, N. R. Cooper, T. Esslinger, and T. Donner, P -band induced self-organization and dynamics with repulsively driven ultracold atoms in an optical cavity, *Phys. Rev. Lett.* **123**, 233601 (2019).
- [39] N. Dogra, M. Landini, K. Kroeger, L. Hruby, T. Donner, and T. Esslinger, Dissipation-induced structural instability and chiral dynamics in a quantum gas, *Science* **366**, 1496 (2019).

- [40] P. Kongkhambut, J. Skulte, L. Mathey, J. G. Cosme, A. Hemmerich, and H. Keßler, Observation of a continuous time crystal, *Science* **377**, 670 (2022).
- [41] X. Li, D. Dreon, P. Zupancic, A. Baumgärtner, A. Morales, W. Zheng, N. R. Cooper, T. Donner, and T. Esslinger, First order phase transition between two centro-symmetric superradiant crystals, *Phys. Rev. Res.* **3**, L012024 (2021).
- [42] D. Dreon, A. Baumgärtner, X. Li, S. Hertlein, T. Esslinger, and T. Donner, Self-oscillating pump in a topological dissipative atom-cavity system, *Nature (London)* **608**, 494 (2022).
- [43] Z. Zhang, D. Dreon, T. Esslinger, D. Jaksch, B. Buca, and T. Donner, Tunable non-equilibrium phase transitions between spatial and temporal order through dissipation, [arXiv:2205.01461](https://arxiv.org/abs/2205.01461).
- [44] P. Nataf, A. Baksic, and C. Ciuti, Double symmetry breaking and two-dimensional quantum phase diagram in spin-boson systems, *Phys. Rev. A* **86**, 013832 (2012).
- [45] D. J. Thouless, Quantization of particle transport, *Phys. Rev. B* **27**, 6083 (1983).
- [46] R. Citro and M. Aidelsburger, Thouless pumping and topology, *Nat. Rev. Phys.* **5**, 87 (2023).
- [47] S. Nakajima, T. Tomita, S. Taie, T. Ichinose, H. Ozawa, L. Wang, M. Troyer, and Y. Takahashi, Topological Thouless pumping of ultracold fermions, *Nature Phys.* **12**, 296 (2016).
- [48] D. Vanderbilt and R. D. King-Smith, Electric polarization as a bulk quantity and its relation to surface charge, *Phys. Rev. B* **48**, 4442 (1993).
- [49] R. Resta, Macroscopic polarization in crystalline dielectrics: The geometric phase approach, *Rev. Mod. Phys.* **66**, 899 (1994).
- [50] D. Xiao, M.-C. Chang, and Q. Niu, Berry phase effects on electronic properties, *Rev. Mod. Phys.* **82**, 1959 (2010).